From Particle Fluctuations to Macroscopic Evolution Equations:
The Case of Exclusion Dynamics ⋆ ⋆⋆

Shenglin Huang[1][0000−0002−7450−6966], Santiago Aguado-Montero[2],
Nicolas Dirr[3][0000−0003−3634−7367], Johannes Zimmer[4][0000−0002−7606−2422], and
Celia Reina[1][0000−0001−9302−3401]

[1] Department of Mechanical Engineering and Applied Mechanics, University of
Pennsylvania, Philadelphia PA 19104, USA
{slhuang, creina}@seas.upenn.edu
[2] Escuela Técnica Superior de Ingeniería, Universidad de Sevilla, Sevilla 41092, Spain
saguado@us.es
[3] School of Mathematics, Cardiff University, Cardiff CF24 4AG, UK
DirrNP@cardiff.ac.uk
[4] Fakultät für Mathematik, Technische Universität München, 85748 Garching,
Germany jz@ma.tum.de

Abstract. We consider the symmetric simple exclusion process in one
dimension as an example of a stochastic particle process exhibiting anoma-
lous diffusion; this process is so slow that the mean-square displacement
of a tagged particle is sub-linear. This implies that the standard mean-
square displacement method (Einstein relation) cannot be applied to
determine the diffusivity for the associated macroscopic equation de-
scribing the hydrodynamic limit. We demonstrate that a recent approach
developed by the authors and collaborators, based on the covariation of
the fluctuations, is applicable to this process and does not only deliver
the transport coefficient, but the entire evolution operator associated
with the formulation of the macroscopic equation as an entropic gradi-
ent flow. Furthermore, the approach relies on fluctuations of the density
field (macroscopic fluctuations) as opposed to particle level data. This
data could in principle be obtained from experimental observations.

Keywords: Anomalous diffusion · Fluctuation-dissipation relation · Fluc-
tuating hydrodynamics.

1 Introduction

Anomalous diffusion is characterised by a nonlinear dependence of the mean
squared displacement (MSD) as a function of time, in contrast with the classical

---

diffusion of Brownian particles, where MSD $\propto t$ (at large times). Examples of anomalous diffusion include sublinear diffusion observed in biological applications, such as diffusion in the cell nuclei and membranes; other examples occur for instance in disordered media, astronomy, fluid mechanics and network theory [10]. A classic paper giving a broad overview on this topic is [5].

Anomalous diffusion poses numerous theoretical difficulties (see, for example, [5]). However, the challenges are also of very practical nature. Simulation of particle processes can quickly become prohibitively expensive. One thus seeks macroscopic descriptions in form of partial differential equations (PDEs). A common procedure is to assume phenomenologically the structure of the governing equation and then determine the transport coefficients appearing in it from particle simulations. Prominent methods to determine diffusion coefficients are Green-Kubo relations (based on time-correlation functions) and Einstein relation (based on the mean square displacement) [7]. However, these methods do not provide information on the structure of the PDE. Furthermore, the Einstein relation has as underlying assumption that the MSD scales linearly with time, MSD $\propto t$, and is thus not directly applicable to anomalous diffusion processes.

In this contribution, we show that an alternative approach developed by some of the authors and their collaborators [6, 9] delivers the full structure of the PDE (and parameters therein) for an example of anomalous diffusion, namely for the symmetric simple exclusion process. More specifically, this approach delivers the operator of the macroscopic evolution equation (in discretised form), written as a gradient flow of the entropy functional, without making further phenomenological assumptions on the macroscopic evolution.

We now explain the *symmetric simple exclusion process* (SSEP) in more detail. In this process, particles sit on a lattice and jump stochastically to one of its neighbouring sites with a constant rate, which can be assumed to be one without loss of generality. The central feature of the process is that such a jump is only possible if the destination site is empty, which results in every site being occupied at most by one particle. If the target site is already occupied, then the particle cannot jump and remains at its current location. Mathematically, the jump rate from a site X to a neighbouring site $\tilde{X}$ can be expressed as $g_{X \to \tilde{X}}(\eta) := \frac{1}{2^d} \eta(X)(1 - \eta(\tilde{X}))$, where d is the dimension of the space (here, $d = 1$), and $\eta(X)$ is zero (one) if site X is empty (occupied); see [8, Section 2.2] for further details. In one space dimension, the resulting process is slow – as in a single-lane motorway, one slow particle is enough to impede the passage of all the other particles behind, effectively blocking them. Thus (albeit the hydrodynamic limit is a linear diffusion equation), the individual particles themselves are *not* following a Brownian motion on a microscopical level [2]. They are slowed down by the exclusion condition, which results in a sublinear power law for the mean square displacement, namely MSD $\propto t^{1/2}$.

The methodology of [6] has been shown to be applicable in this context, though, to determine the governing transport coefficient only. In this contribution, we show that the method can be extended using the approach of [9] to

determine the full macroscopic evolution numerically from particle simulations, assuming the governing entropy is known.

The key requirement for the application of the strategy outlined in [9] is that the macroscopic evolution is a gradient flow, and that fluctuations around such limit are Gaussian. This means that the density evolution has the following thermodynamic structure in the limit of infinitely many particles

$$\partial_t \rho = \mathcal{K}(\rho) \frac{\delta \mathcal{S}}{\delta \rho}(\rho) =: \mathcal{K}_\rho \frac{\delta \mathcal{S}}{\delta \rho}(\rho), \tag{1}$$

where $\mathcal{K}_\rho$ is a symmetric operator, and $\frac{\delta \mathcal{S}}{\delta \rho}$ is the variational derivative of the entropy functional, while for large but finite number of particles N, the evolution shall be formally described by the stochastic partial differential equation of the form

$$\partial_t \rho = \mathcal{K}(\rho) \frac{\delta S(\rho)}{\delta \rho} + \sqrt{\frac{C}{N}} \sqrt{2\mathcal{K}(\rho)} \dot{W}_{t,x}, \tag{2}$$

with $\dot{W}_{t,x}$ a space-time white noise, and C a constant such that $\epsilon = C/N$ is the individual lattice site volume. Equation (2) highlights a very important relation between fluctuations and dissipation: the *same* operator $\mathcal{K}$ appears in the deterministic (macroscopic) part and in the fluctuations. This important connection precisely lies at the core of the approach in [9].

For the symmetric simple exclusion process, the macroscopic (hydrodynamic) limit under parabolic scaling is known to be the linear diffusion equation $\partial_t \rho = \Delta \rho$ [8, Section 2.2]. Yet, the linear nature disguises nonlinear features that are apparent when written in the thermodynamic form, given in Eq. (1). Indeed, the macroscopic equation is a gradient flow of the entropy (further details in Section 2), with S being the *mixing entropy*, i.e.,

$$\mathcal{S}(\rho) = - \int [\rho \log \rho + (1 - \rho) \log(1 - \rho)] \, dx \tag{3}$$

in dimensionless form, and $\mathcal{K}$ the operator $\mathcal{K}(\rho)\xi := -\operatorname{div}(\rho(1 - \rho)\nabla\xi)$, i.e.,

$$\partial_t \rho = \Delta \rho = -\operatorname{div}(\rho(1 - \rho)\nabla \frac{\delta \mathcal{S}}{\delta \rho}(\rho)) = \mathcal{K}_\rho \frac{\delta \mathcal{S}}{\delta \rho}(\rho). \tag{4}$$

2   Gradient Flow Structure of the SSEP

In this section, we explain why the formulation (4) is a gradient flow. We include this calculation as the setting does not seem to be described in the literature, though readers with a focus on the computational aspects can safely skip this section.

We show that (4) is the steepest descent in a weighted version of the standard L^2 Wasserstein geometry. The argument is sketched adapting ideas by Benamou and Brenier [3]; see also [1]. In this context, a *gradient flow* of a functional $\mathcal{S}$ is defined as the evolution

$$(\partial_t \rho, s_2)_{\mathcal{K}^{-1}} = \int \frac{\delta \mathcal{S}}{\delta \rho} s_2 \, dx, \tag{5}$$

where the geometry of the gradient evolution is defined by an inner product, here symbolically denoted $\mathcal{K}^{-1}$; Eq. (5) is a weak formulation in the sense that it has to be satisifed for all suitable test functions s_2.

We now define the inner product in (5). For the SSEP, the evolution takes place on the space of probability measures with bounded Lebesgue density $0 < \rho < 1$ (almost surely). For such measures, we define formally an inner product on the tangent space,

$$(s_1, s_2)_{\mathcal{K}^{-1}} := \int \frac{\rho}{1 - \rho} \nabla \Psi_1 \nabla \Psi_2 \, \mathrm{d}x, \tag{6}$$

where $s_j = -\operatorname{div}(\rho \nabla \Psi_j)$ for $j = 1, 2$. (The tangent space can be interpreted as time derivatives satisfying the continuity equation.) The last equation also defines the class of test functions in Eq. (5).

We now compute the expressions of the gradient flow evolution for the SSEP. On one hand, we find with undetermined Ψ_1 and Ψ_2 and

$$\partial_t \rho = -\operatorname{div}(\rho \nabla \Psi_1) \text{ and } s_2 = -\operatorname{div}(\rho \nabla \Psi_2) \tag{7}$$

for the expression on the left of (5)

$$(\partial_t \rho, s_2)_{\mathcal{K}^{-1}} = \int \rho \nabla \Psi_1 \frac{1}{1 - \rho} \nabla \Psi_2 \, \mathrm{d}x. \tag{8}$$

On the other hand, the expression of the right of (5) becomes with the mixing entropy (3)

$$\int \frac{\delta \mathcal{S}}{\delta \rho} s_2 \, \mathrm{d}x = -\int \log\left(\frac{\rho}{1 - \rho}\right) \operatorname{div}(\rho \nabla \Psi_2) \, \mathrm{d}x$$
$$= \int \rho \nabla \log\left(\frac{\rho}{1 - \rho}\right) \nabla \Psi_2 \, \mathrm{d}x = \int \nabla \rho \frac{1}{1 - \rho} \nabla \Psi_2 \, \mathrm{d}x. \tag{9}$$

As, in the absence of topological obstructions, any gradient vector field ∇f can be written in the form

$$\nabla f = \frac{1}{1 - \rho} \nabla \Psi_2 \tag{10}$$

(by solving $\operatorname{div}\left(\frac{1}{1-\rho} \nabla \Psi_2\right) = \Delta f$), the combination of (8) and (9) yields

$$\int \rho \nabla \Psi_1 \, \nabla f \, \mathrm{d}x = \int \nabla \rho \nabla f \, \mathrm{d}x.$$

With the first continuity equation in (8) and integration by parts, this becomes

$$\int \partial_t \rho f \, \mathrm{d}x = \int \nabla \rho \nabla f \, \mathrm{d}x,$$

which is the weak form of the hydrodynamic limit (4) associated with the SSEP.

For the SSEP, we call Eq. (6) the *thermodynamic metric*. It is a weighted version of the classic Wasserstein metric.

We notice that there are different ways to obtain the linear diffusion equation (4), $\partial_t \rho = \Delta \rho$ as gradient flow. For example, we can use the standard Wasserstein metric and the standard (Boltzmann) entropy $\mathcal{S} = -\int \rho \log \rho \, dx$ (see, for example, [1]), or the thermodynamic metric (6) of the SSEP and the mixing entropy (3). This shows an advantage of the entropic gradient flow formulation: here the differences between different proceses become visible, even if they have the same macroscopic limit. For example, Brownian particles define the classic (Boltzmann) entropy gradient flow, and the SSEP defines the thermodynamic flow of the mixing entropy. Even if the hydrodynamic limit of the two processes is the same, their fluctuations are different, as evident from Eq. (2). The entropy-metric pair also records these differences.

3   Computational Framework

3.1   Discretisation of the Dissipative Operator

The partial differential equation (4) and the operator $\mathcal{K}_\rho$ that the PDE encodes are infinite dimensional objects. Thus, their full characterisation from particle level data either requires infinite amount of data, which is of course unattainable from numerical simulations, or, alternatively, optimal fits from a finite library of infinite dimensional operators. To avoid the phenomenology of the latter approach, we here use particle data to physically infer a discretised version of the dissipative operator (i.e., now a finite dimensional object), as previously proposed by the authors in [9]. Specifically, we consider a finite element approximation scheme of the density field ρ and the thermodynamic driving force $F := \delta S / \delta \rho$ of the form,

$$\rho(x,t) \approx \sum_a \rho_a(t)\gamma_a(x), \quad \text{and} \quad F(x,t) \approx \sum_a F_a(t)\gamma_a(x), \tag{11}$$

where $\{\gamma_a(x)\}$ is a basis of functions with local support. These satisfy the so-called partition of unity $\sum_a \gamma_a(x) = 1$, linear field reproduction $\sum_a \gamma_a(x)x_a = x$ and Kronecker-Delta property $\gamma_a(x_b) = \delta_{ab}$ (the latter is particularly convenient when numerically solving the PDE with Dirichlet boundary conditions). For the case of SSEP, linear finite element shape functions provide sufficient regularity to approximate the above fields and are here chosen for their simplicity. For a regular mesh with nodal spacing Δx in one dimension, such shape functions can be written as

$$\gamma_a(x) = \frac{1}{\Delta x} \max(|x - x_a|, 0). \tag{12}$$

Substituting the approximation given in Eq. (11) into the evolution equation Eq. (4), and further testing it with a shape function γ_b, one obtains the weak form of the evolution equations,

$$\sum_a \langle \gamma_a, \gamma_b \rangle \frac{\partial \rho_a}{\partial t} = \sum_a \langle \mathcal{K}_\rho \gamma_a, \gamma_b \rangle F_a, \quad \text{for all } b, \tag{13}$$

where the bracket $\langle \cdot, \cdot \rangle$ denotes the integral inner product in the L^2 space. The resulting matrix $\langle \mathcal{K}_\rho \gamma_a, \gamma_b \rangle$ represents the discretised dissipative operator, which we will seek to estimate from particle data, with the strategy outlined in Section 3.2. We note that for processes satisfying conservation of mass, as the SSEP of interest here, the discretised operator entries should satisfy the constraint

$$\sum_b \langle \mathcal{K}_\rho \gamma_a, \gamma_b \rangle = 0. \tag{14}$$

Equivalently, this constraint can be written as $\sum_b \langle \mathcal{K}_\rho \gamma_b, \gamma_a \rangle = 0$ for symmetric operators, as the one associated to SSEP or any other purely dissipative processes with the structure of Eq. (1).

Despite the finite-dimensional nature of $\langle \mathcal{K}_\rho \gamma_a, \gamma_b \rangle$, this operator is, *a priori*, a function of the entire density profile, or, for the already assumed finite element approximation, a function of all the nodal density values. Consequently, its domain is extremely vast and dependent on the specific simulation domain, rendering the sought-after approach computationally intractable and of limited generality. Yet, many physical processes, such as SSEP are governed by local operators. This property, combined with the fact that the chosen basis functions have local support, implies that $\langle \mathcal{K}_\rho \gamma_a, \gamma_b \rangle$ is only non-zero for the cases where node a is equal or near to node b (concretely, $a = \{b-1, b, b+1\}$), and that only the local density profile is needed to determine the discretised operator. This important observation allows us to approximate the density profile by means of a Taylor expansion, and rewrite Eq. (13) as

$$\sum_a \langle \gamma_a, \gamma_b \rangle \frac{\partial \rho_a}{\partial t} \approx \sum_{a \in \{b-1, b, b+1\}} \left\langle \mathcal{K}_{\left(\rho_a + \nabla \rho|_a (x - x_a) + \ldots\right)} \gamma_a, \gamma_b \right\rangle F_a. \tag{15}$$

For SSEP, we will truncate the Taylor expansion after the liner term, rendering $\langle \mathcal{K}_\rho \gamma_a, \gamma_b \rangle$ a function of only two variables: ρ_a and $\nabla \rho|_a$. From a practical perspective, this implies that only linear profiles, encompassing different densities and gradients, are to be simulated to characterise the discretised operator from the associated particle data.

Once the discrete operator has been estimated, this may then be used to simulate the evolution of arbitrary initial profiles, i.e., not necessarily linear ones. For this, we will use a forward Euler time discretisation scheme, and rewrite Eq. (15) as

$$\mathbf{M} \frac{\boldsymbol{\rho}^{i+1} - \boldsymbol{\rho}^i}{\Delta t} = \mathbf{K}^i \mathbf{F}^i. \tag{16}$$

where the superscript "i" denotes the time step t^i, and all quantities have been written in the form of vectors and matrices. Specifically, $\boldsymbol{\rho}^i = \left(\rho_a^i\right)_{N_\gamma \times 1}$ is the vector of densities at the nodal positions, $\boldsymbol{\nabla} \boldsymbol{\rho}^i = \left(\nabla \rho|_a^i\right)_{N_\gamma \times 1}$ is the vector of density gradients, and $\mathbf{F}^i = \mathbf{F}^i \left(\boldsymbol{\rho}^i\right) = \left(F_a^i \left(\boldsymbol{\rho}^i\right)\right)_{N_\gamma \times 1}$ is the vector of thermodynamic driving forces, where N_γ is the number of basis functions. Furthermore, the matrix forms of $\mathbf{M}$ (independent of time) and the dissipative operator $\mathbf{K}^i$ read

$$\mathbf{M} = \left(\langle \gamma_a, \gamma_b \rangle\right)_{N_\gamma \times N_\gamma} = \varDelta x \begin{pmatrix} 2/3 & 1/6 & 0 & \cdots & 1/6 \\ 1/6 & 2/3 & 1/6 & \ddots & \vdots \\ 0 & 1/6 & \ddots & \ddots & 0 \\ \vdots & \ddots & \ddots & \ddots & 1/6 \\ 1/6 & \cdots & 0 & 1/6 & 2/3 \end{pmatrix}_{N_\gamma \times N_\gamma}, \qquad (17)$$

$$\mathbf{K}^i = \mathbf{K}^i\left(\boldsymbol{\rho}^i, \boldsymbol{\nabla}\boldsymbol{\rho}^i\right) = \left(K_{ba}^i\right)_{N_\gamma \times N_\gamma}$$

$$= \begin{pmatrix} K_{11}^i & K_{12}^i & 0 & \cdots & & K_{1N_\gamma}^i \\ K_{21}^i & K_{22}^i & K_{23}^i & \ddots & & \vdots \\ 0 & K_{32}^i & \ddots & \ddots & & 0 \\ \vdots & \ddots & \ddots & \ddots & & K_{N_\gamma-1,N_\gamma}^i \\ K_{N_\gamma 1}^i & \cdots & 0 & K_{N_\gamma,N_\gamma-1}^i & K_{N_\gamma N_\gamma}^i \end{pmatrix}_{N_\gamma \times N_\gamma}$$

$$= \begin{pmatrix} K^0(X_1^i) & K^p(X_2^i) & 0 & \cdots & & K^m(X_{N_\gamma}^i) \\ K^m(X_1^i) & K^0(X_2^i) & K^p(X_3^i) & \ddots & & \vdots \\ 0 & K^m(X_2^i) & \ddots & \ddots & & 0 \\ \vdots & \ddots & \ddots & \ddots & & K^p(X_{N_\gamma}^i) \\ K^p(X_1^i) & \cdots & 0 & K^m(X_{N_\gamma-1}^i) & K^0(X_{N_\gamma}^i) \end{pmatrix}_{N_\gamma \times N_\gamma}, \qquad (18)$$

where K^0, K^p and K^m represent the three operator entries $\langle \mathcal{K}_\rho \gamma_a, \gamma_b \rangle = K_{ba}$ with $a = b-1, b, b+1$, respectively, $X_a^i = (\rho_a^i, \nabla\rho|_a^i)$, and the periodic boundary conditions have been considered.

3.2 Fluctuation-Dissipation Statement to Compute the Discretised Operator from Density Fluctuations

For any given density profile, $\langle \mathcal{K}_\rho \gamma_a, \gamma_b \rangle$ can be computed from the covariation of the rescaled local density fluctuation as [9]

$$\langle \mathcal{K}_\rho \gamma_a, \gamma_b \rangle = \lim_{h \searrow 0} \frac{1}{2h} \mathbb{E}\left[\left(Y_{\gamma_a}(t_0 + h) - Y_{\gamma_a}(t_0)\right) \cdot \left(Y_{\gamma_b}(t_0 + h) - Y_{\gamma_b}(t_0)\right)\right], \quad (19)$$

where t_0 is an arbitrary initial time that does not affect the result for the operator entries as long as the system has reached a local equilibrium, $\mathbb{E}[\cdot]$ represents the expectation, and Y_γ are local rescaled density fluctuations, defined as $Y_\gamma = \lim_{\epsilon \to 0} \langle \rho_\epsilon - \rho, \gamma \rangle / \sqrt{\epsilon}$ with $\rho = \mathbb{E}[\rho_\epsilon]$. In practice, the particle system is of course simulated with a finite number of sites, and thus the limit as $\epsilon \to 0$ in Y_γ is numerically approximated. Similarly, the right hand side of Eq. (19) is

computed for a finite time step h, that is sufficiently small to capture the limit numerically, yet, sufficiently large for the particle system to exhibit some particle jumps. Finally, the expectation in this same equation will be approximated as the ensemble average over many but finite realisations of macroscopically identical density profiles.

3.3   Polynomial Regression of the Discretised Operator

Equation (19) will enable the calculation of the discrete operator

$$K_{ba} = \left\langle \mathcal{K}_{\left(\rho_a + \nabla \rho|_a (x - x_a)\right)} \gamma_a, \gamma_b \right\rangle$$

for a finite set of linear profiles, resulting in a discrete space V_{discr} of ρ_a and $\nabla \rho|_a$. Yet, its use in Eq. (15) to simulate the evolution of arbitrary density profiles will require evaluating K_{ba} at different density and density gradient values, for which a suitable interpolation scheme is therefore needed. Towards this goal, we recall that the three operator entries K_{ba} with $a \in \{b-1, b, b+1\}$ should satisfy the constraint given by Eq. (14) in order for the evolution to be mass preserving. Although such identity may not be exactly satisfied for the particle-inferred operator in V_{discr}, we here perform a polynomial regression on such data that, by construction, exactly satisfies the conservation constraint. More specifically, denoting by $\phi_j(X)$ $(j = 1, 2, \ldots, n)$ the fitting basis, with $X = (\rho, \nabla \rho)$, we approximate the three non-zero entries of the discretised operator as

$$K^0 = \sum_{j=1}^{n} a_j^0 \phi_j(X), \tag{20}$$

$$K^m = \sum_{j=1}^{n} a_j^m \phi_j(X), \tag{21}$$

$$K^p = -K^0 - K^m = -\sum_{j=1}^{n} \left(a_j^0 + a_j^m \right) \phi_j(X), \tag{22}$$

where K^0, K^m and K^p have been defined after Eq. (18). For simplicity, we use polynomials up to order-k as the basis functions, i.e., $\phi_j(X) \in \{1, \rho, \nabla \rho, \rho^2, \rho \nabla \rho, (\nabla \rho)^2, \ldots, \rho^k, \ldots, (\nabla \rho)^k\}$. Specifically, we will use $k = 4$ to fit the discrete operator data for SSEP.

Towards the goal of finding the optimal fitting parameter a_j^0 and a_j^m, we denote the data points from the numerical simulation as $\{X_i^0, K_i^0\}$ with $i = 1, \ldots, N_0$ for the diagonal entry K_{bb}, $\{X_i^m, K_i^m\}$ with $i = 1, \ldots, N_m$ for the sub-diagonal entry $K_{b,b-1}$, and $\{X_i^p, K_i^p\}$ with $i = 1, \ldots, N_p$ for the super-diagonal entry $K_{b,b+1}$, where N_0, N_m, N_p are the number of data points for the three entries, respectively. We then define the loss function L as the sum of the least

square error for all three entries, i.e.,

$$L = \frac{1}{2} \sum_{i=1}^{N_0} \left[\sum_{j=1}^{n} \phi_j(X_i^0) a_j^0 - K_i^0 \right]^2 + \frac{1}{2} \sum_{i=1}^{N_m} \left[\sum_{j=1}^{n} \phi_j(X_i^m) a_j^m - K_i^m \right]^2$$

$$+ \frac{1}{2} \sum_{i=1}^{N_p} \left[-\sum_{j=1}^{n} \phi_j(X_i^p) \left(a_j^0 + a_j^m \right) - K_i^p \right]^2. \quad (23)$$

The minimum of the loss function can be analytically computed by setting its partial derivatives with respect to $\mathbf{a}^0$ and $\mathbf{a}^m$ to zero, i.e.,

$$\frac{\partial L}{\partial \mathbf{a}^0} = \mathbf{\Phi}^{0\mathbf{T}} \left(\mathbf{\Phi}^0 \mathbf{a}^0 - \mathbf{K}^0 \right) + \mathbf{\Phi}^{p\mathbf{T}} \left[\mathbf{\Phi}^p \left(\mathbf{a}^0 + \mathbf{a}^m \right) + \mathbf{K}^p \right] = \mathbf{0}, \quad (24)$$

$$\frac{\partial L}{\partial \mathbf{a}^m} = \mathbf{\Phi}^{m\mathbf{T}} \left(\mathbf{\Phi}^m \mathbf{a}^m - \mathbf{K}^m \right) + \mathbf{\Phi}^{p\mathbf{T}} \left[\mathbf{\Phi}^p \left(\mathbf{a}^0 + \mathbf{a}^m \right) + \mathbf{K}^p \right] = \mathbf{0}. \quad (25)$$

We remark that the above equations use the matrix/vector forms for the fitting parameters $\mathbf{a}^0 = (a_j^0)_{n \times 1}$, $\mathbf{a}^m = (a_j^m)_{n \times 1}$, the operator entries $\mathbf{K}^0 = (K_j^0)_{N_0 \times 1}$, $\mathbf{K}^m = (K_j^m)_{N_m \times 1}$, $\mathbf{K}^p = (K_j^p)_{N_p \times 1}$, and the basis functions $\mathbf{\Phi}^0 = (\phi_j(X_i^0))_{N_0 \times n}$, $\mathbf{\Phi}^m = (\phi_j(X_i^m))_{N_m \times n}$, $\mathbf{\Phi}^p = (\phi_j(X_i^p))_{N_p \times n}$. Denoting

$$\mathbf{\Phi} = \begin{pmatrix} \mathbf{\Phi}^{0\mathbf{T}} \mathbf{\Phi}^0 + \mathbf{\Phi}^{p\mathbf{T}} \mathbf{\Phi}^p & \mathbf{\Phi}^{p\mathbf{T}} \mathbf{\Phi}^p \\ \mathbf{\Phi}^{p\mathbf{T}} \mathbf{\Phi}^p & \mathbf{\Phi}^{m\mathbf{T}} \mathbf{\Phi}^m + \mathbf{\Phi}^{p\mathbf{T}} \mathbf{\Phi}^p \end{pmatrix},$$

$$\mathbf{a} = \begin{pmatrix} \mathbf{a}^0 \\ \mathbf{a}^m \end{pmatrix}, \quad \text{and} \quad \mathbf{b} = \begin{pmatrix} \mathbf{\Phi}^{0\mathbf{T}} \mathbf{K}^0 - \mathbf{\Phi}^{p\mathbf{T}} \mathbf{K}^p \\ \mathbf{\Phi}^{m\mathbf{T}} \mathbf{K}^m - \mathbf{\Phi}^{p\mathbf{T}} \mathbf{K}^p \end{pmatrix}, \quad (26)$$

Equations (24)–(25) can be equivalently written in compact form as

$$\mathbf{\Phi} \mathbf{a} = \mathbf{b}, \quad (27)$$

delivering a simple linear system of equations from which the fitting parameters $\mathbf{a}$ can be obtained. Alternatively, a constrained least-square solver available in some commercial packages could be used to find the optimal fitting parameters.

4   Numerical Results

4.1   Discretised Operator from Particle Fluctuations

In order to compute the operator entries numerically from density fluctuation using Eq. (19), we use the lattice kinetic Monte-Carlo (KMC) method [4], implemented in C++, to simulate the particle jumps for SSEP over a unit interval with $N_{\text{sites}} = 5000$ sites (i.e., $\epsilon = 1/5000$). We perform simulations with 43 different initial linear (or piecewise linear) density profiles, which results in the discrete space V_{discr} shown in Fig. 1, with data points within the range of $\rho \in [0.05, 0.95]$ and $\nabla \rho \in [-3, 3]$.
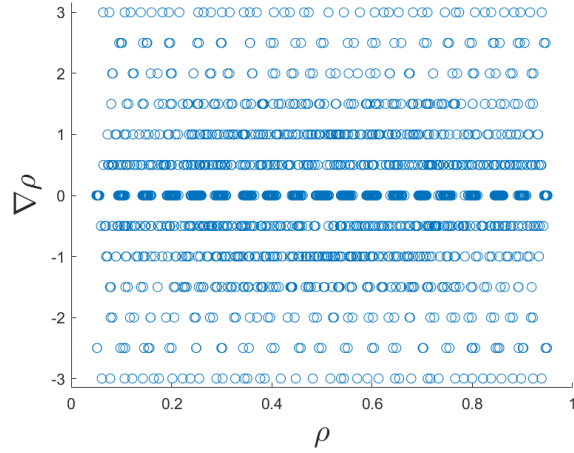
Fig. 1. The probed discrete data space V_{discr} of $(\rho, \nabla\rho)$ used to evaluate the discretised operator.

For each initial profile, we perform $R = 10^5$ realisations using the strategy of [6] aimed at partially alleviating the computational burden associated to the equilibration time (this strategy requires additional parameters, which are here chosen as $R_1 = 50$, $R_2 = 2000$, equilibration time $t_{prep} - t_{ini} = 4 \times 10^{-6}$ and randomisation time $t_0 - t_{prep} = 4 \times 10^{-9}$). The actual time interval over which the covariation in density fluctuations are computed is $h = 4 \times 10^{-10}$. Additionally, $N_\gamma = 50$ shape functions are used to discretise the macroscopic domain.

The results for the three operator entries $\langle \mathcal{K}_\rho \gamma_a, \gamma_b \rangle$ with $a \in \{b-1, b, b+1\}$ are shown in Figs. 2(a)–(c) (blue circles) together with the analytical surfaces, obtained by performing a Taylor expansion on x_a as

$$\langle \mathcal{K}_\rho \gamma_b, \gamma_b \rangle = \langle m \nabla\gamma_b, \nabla\gamma_b \rangle = 2\frac{m_b}{\Delta x} + \frac{1}{3}\frac{\partial^2 m}{\partial x^2}\Big|_b \Delta x + O(\Delta x^2), \tag{28}$$

$$\langle \mathcal{K}_\rho \gamma_{b-1}, \gamma_b \rangle = \langle m \nabla\gamma_{b-1}, \nabla\gamma_b \rangle = -\frac{m_{b-1}}{\Delta x} - \frac{1}{2}\frac{\partial m}{\partial x}\Big|_{b-1} - \frac{1}{6}\frac{\partial^2 m}{\partial x^2}\Big|_{b-1} \Delta x$$
$$+ O(\Delta x^2), \tag{29}$$

$$\langle \mathcal{K}_\rho \gamma_{b+1}, \gamma_b \rangle = \langle m \nabla\gamma_{b+1}, \nabla\gamma_b \rangle = -\frac{m_{b+1}}{\Delta x} + \frac{1}{2}\frac{\partial m}{\partial x}\Big|_{b+1} - \frac{1}{6}\frac{\partial^2 m}{\partial x^2}\Big|_{b+1} \Delta x$$
$$+ O(\Delta x^2), \tag{30}$$

with

$$m_a = \rho_a(1 - \rho_a), \ \frac{\partial m}{\partial x}\Big|_a = \nabla\rho|_a (1 - 2\rho_a), \ \text{and} \ \frac{\partial^2 m}{\partial x^2}\Big|_a = -2(\nabla\rho|_a)^2 + O(\nabla\rho^2). \tag{31}$$

The diagonal entry K_{bb} is symmetric with respect to $\rho = 0.5$ and is independent with $\nabla\rho$, while the two off-diagonal entries are non-symmetric and have
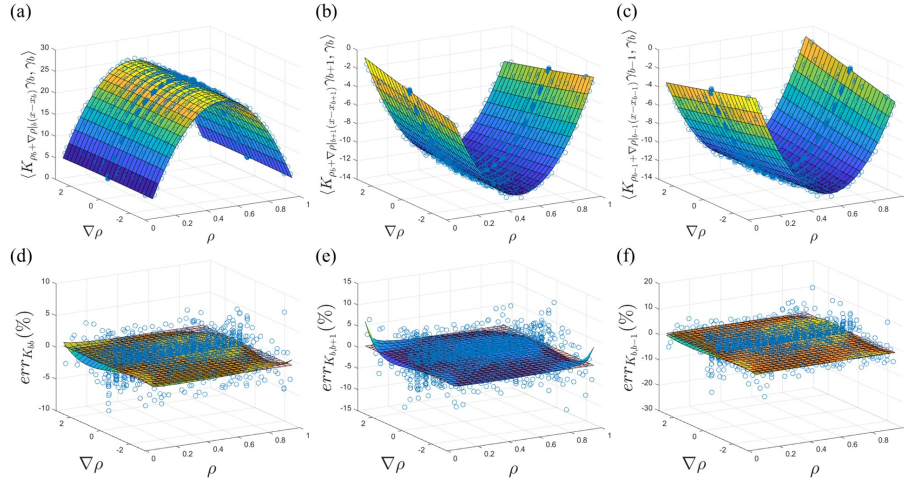
Fig. 2. (a–c) Numerical results (blue circles) for the discretised operator entries $\left\langle \mathcal{K}_{\left(\rho_a + \nabla \rho|_a (x - x_a)\right)} \gamma_a, \gamma_b \right\rangle$ with $a \in \{b-1, b, b+1\}$ as a function of density ρ and density gradient $\nabla \rho$ (at node a) in V_{discr}, shown in Fig. 1. The analytical predictions (smooth surfaces) based on Eqs. 28–30 are jointly shown. (d–f) Corresponding relative errors (in %), denoted as $err_{K_{ba}}$ with $a \in \{b-1, b, b+1\}$, for the numerical results, between the data and analytical results (blue circles) together with the relative errors for the polynomial regression of data (smooth surface with non-zero relative error).

an opposite dependence due to the mass conservation constraint. The relative error between the data points and the analytical predictions is quantified in Figs. 2(d)–(f), where the relative error of the fit, following Section 3.3, is also shown. As it may be observed in the figure, the fourth order polynomial regression with mass conservation strictly enforced significantly decreases the error: while the standard deviation of the relative errors of the original data points for three entries $K_{bb}, K_{b,b+1}$ and $K_{b,b-1}$ are 1.4%, 2.3% and 2.5%, respectively, these get reduced to 0.27%, 0.44% and 0.31%, respectively, for the polynomial fit. Similarly, the maximum relative errors decrease from 7.9%, 12.7% and 21.6%, to 2.6%, 5.7% and 3.8%. We remark that the relative errors are larger near $\rho = 0$ and $\rho = 1$, where the analytical values of operator entries are close to 0, and the relative errors thus become singular. Overall, the numerical strategy outlined in this section delivers a high accuracy for the discretised dissipative operator governing the simple exclusion process.

4.2   Macroscopic Simulation

We now test the capability of the particle-inferred operator to predict the density evolution for an arbitrary initial profile. Concretely, we consider an initial density $\rho(x, 0) = 0.5 - 0.3 \cos(4\pi x)$ over the unit interval $x \in [0, 1]$, discretised with $N_\gamma = 50$ shape functions (i.e., $\Delta x = 1/N_\gamma = 0.02$). This profile is evolved

using the forward Euler scheme described in Eq. (16) with $\Delta t = \Delta x^2/1000$, the discrete operator obtained in Section 4.1 and the analytical driving force, given by the entropy in Eq. (3). Periodic boundary conditions are considered, and the system is evolved till almost reaching an equilibrium state with a flat density profile at the average initial density.

Snapshots of the evolution are represented in Fig. 3, together with the analytic PDE (with identical spatio-temporal discretisation, and discretised operator given by Eqs. (28)–(31)), and the average over multiple realisations of long-time KMC simulations. Due to the large computational cost of these KMC simulations, these are performed using $N_{\text{sites}} = 1000$ sites and averaging over $R = 200$ realisations (we recall that the discretised operator was inferred from particle simulations using $N_{\text{sites}} = 5000$). The numerical results depict an excellent agreement between the three curves, making them almost indistinguishable in the figure.
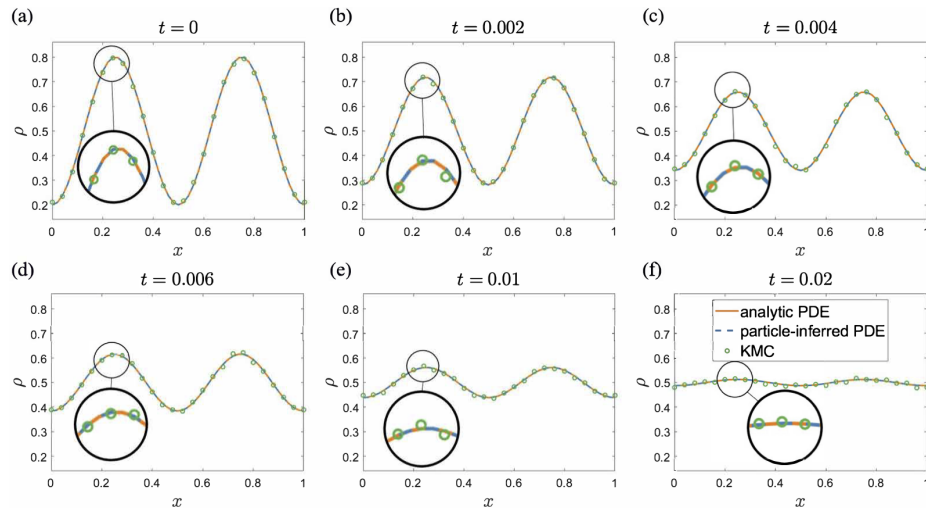

Fig. 3. Snapshots of the density evolution for the symmetric simple exclusion process at times $t = 0$ (a), 0.002 (b), 0.004 (c), 0.006 (d), 0.01(e), and 0.02 (f). Such evolution is computed with three different strategies: PDE with analytic operator, PDE with particle-inferred operator, and long-time KMC simulations.

The present contribution therefore shows that the computational strategy of [9] is able to extract the dissipative operator for the symmetric simple exclusion process, an anomalous diffusion process, and hence, it can be used to predict the non-equilibrium macroscopic evolution of arbitrary initial profiles.

References

1. Adams, S., Dirr, N., Peletier, M., Zimmer, J.: Large deviations and gradient flows. Philos. Trans. R. Soc. Lond. Ser. A Math. Phys. Eng. Sci. **371**(2005), 20120341

(2013). https://doi.org/10.1098/rsta.2012.0341

2. Arratia, R.: The motion of a tagged particle in the simple symmetric exclusion system on **Z**. Ann. Probab. **11**(2), 362–373 (1983). https://doi.org/10.1214/aop/1176993602

3. Benamou, J.D., Brenier, Y.: A computational fluid mechanics solution to the Monge-Kantorovich mass transfer problem. Numer. Math. **84**(3), 375–393 (2000). https://doi.org/10.1007/s002110050002

4. Bortz, A.B., Kalos, M.H., Lebowitz, J.L.: A new algorithm for Monte Carlo simulation of Ising spin systems. J. Computational Phys. **17**(1), 10–18 (1975). https://doi.org/10.1016/0021-9991(75)90060-1

5. Bouchaud, J.P., Georges, A.: Anomalous diffusion in disordered media: statistical mechanisms, models and physical applications. Phys. Rep. **195**(4–5), 127–293 (1990). https://doi.org/10.1016/0370-1573(90)90099-N

6. Embacher, P., Dirr, N., Zimmer, J., Reina, C.: Computing diffusivities from particle models out of equilibrium. Proc. Roy. Soc. London Ser. A **474**(2212) (2018). https://doi.org/10.1098/rspa.2017.0694

7. Frenkel, D., Smit, B.: Understanding molecular simulation: From algorithms to applications. 2nd edn. Academic Press (2001)

8. Kipnis, C., Landim, C.: Scaling limits of interacting particle systems, Grundlehren der Mathematischen Wissenschaften [Fundamental Principles of Mathematical Sciences], vol. 320. Springer-Verlag, Berlin (1999)

9. Li, X., Dirr, N., Embacher, P., Zimmer, J., Reina, C.: Harnessing fluctuations to discover dissipative evolution equations. J. Mech. Phys. Solids **131**, 240–251 (2019). https://doi.org/10.1016/j.jmps.2019.05.017

10. Oliveira, F.A., Ferreira, R.M.S., Lapas, L.C., Vainstein, M.H.: Anomalous diffusion: A basic mechanism for the evolution of inhomogeneous systems. Front. Phys. **7**, 18 (2019). https://doi.org/10.3389/fphy.2019.00018

11. Öttinger, H.C.: Beyond equilibrium thermodynamics. Wiley Online Library (2005)